Langmuir

Article

pubs.acs.org/Langmuir

Directing Cluster Formation of Au Nanoparticles from Colloidal Solution

Sarah M. Adams,[†] Salvatore Campione,[‡] Filippo Capolino,[‡] and Regina Ragan*,[†]

[†]Department of Chemical Engineering and Materials Science, University of California, Irvine, Irvine, California 92697, United States

[‡]Department of Electrical Engineering and Computer Science, University of California, Irvine, Irvine, California 92697, United States

Supporting Information

ABSTRACT: Discrete clusters of closely spaced Au nanoparticles can be utilized in devices from photovoltaics to molecular sensors because of the formation of strong local electromagnetic field enhancements when illuminated near their plasmon resonance. In this study, scalable, chemical self-organization methods are shown to produce Au nanoparticle clusters with uniform nanometer interparticle spacing. The performance of two different methods, namely electrophoresis and diffusion, for driving the attachment of Au nanoparticles using a chemical cross-linker on chemically patterned domains of polystyrene-*block*-poly(methyl methacrylate) (PS-*b*-PMMA) thin films are evaluated. Significantly, electrophoresis is found to produce similar surface coverage as diffusion in 1/6th of the processing time with an ∼2-fold increase in the number of Au nanoparticles forming clusters. Furthermore, average interparticle spacing within Au nanoparticle clusters was found to decrease from 2−7 nm for diffusion deposition to approximately 1−2 nm for electrophoresis deposition, and the latter method exhibited better uniformity with most clusters appearing to have about 1 nm spacing between nanoparticles. The advantage of such fabrication capability is supported by calculations of local electric field enhancements using electromagnetic full-wave simulations from which we can estimate surface-enhanced Raman scattering (SERS) enhancements. In particular, full-wave results show that the maximum SERS enhancement, as estimated here as the fourth power of the local electric field, increases by a factor of 100 when the gap goes from 2 to 1 nm, reaching values as large as 10^{10}, strengthening the usage of electrophoresis versus diffusion for the development of molecular sensors.

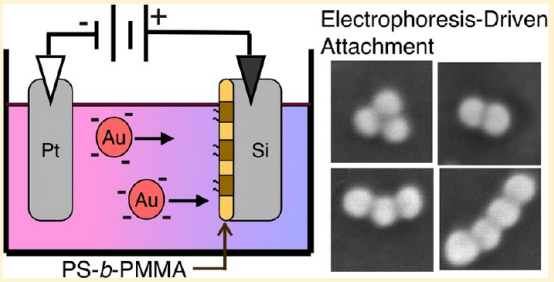

INTRODUCTION

It has long been established that local electromagnetic field enhancements observed in noble metal nanoparticles, as a result of excitation at the plasmon resonance, increase as nanoparticles electromagnetically couple with nanometer scale interparticle spacing.[1,2] Significant advances in controlling the nanostructure and local composition via chemical synthesis[3−6] coupled with theoretical understanding of electromagnetic coupling[2,7−12] allows for tuning optical properties across the electromagnetic spectrum. While these plasmonic systems have been demonstrated to have numerous applications such as molecular sensors and efficiency-enhanced photovoltaics, scalable methods to produce nanostructures over a large area on surfaces using processes that are nonprohibitive in cost are still challenging.

Here, using chemical assembly, colloidal metal nanostructures are fabricated on substrates with nanometer scale interparticle spacing over sample areas of 1 cm^2. This permits the versatility achievable in chemical synthesis to be utilized on surfaces. Furthermore, chemical assembly relies on solution methods and avoids costly lithographic techniques for nanostructure formation on substrates while at the same time achieving nanometer interparticle spacing, which is unachievable even with electron beam lithography.[13] Assembly from colloidal solution as performed here allows for attachment of complex nanostructures, including core−shell and faceted structures,[14] to patterned chemical domains that can achieve large area ordering when integrated with larger-scale lithographic methods such as with graphoepitaxial patterning[15] or patterning chemical domains using UV lithography.[16] In the case of diblock copolymers thin films, morphology is variable by altering the copolymer molecular weights,[17,18] and ordered surface patterns have been produced using field-assisted patterning[19] and solvent evaporation.[20] Planar assemblies of isolated Au nanoparticles and/or clusters can be used in a number of applications, including highly sensitive molecular sensors based on SERS[21−23] and increased efficiency in photovoltaic devices.[24,25] Inexpensive production of dense planar assemblies of discrete clusters of nanoparticles would contribute greatly to developing plasmonic devices.

In this paper we compare two methods of directing nanoparticle deposition in solution on PMMA domains of polystyrene-*block*-poly(methyl methacrylate) (PS-*b*-PMMA) thin films: diffusion and electrophoresis. Diffusion deposition

Received: January 2, 2013
Revised: February 27, 2013
Published: March 8, 2013

   dx.doi.org/10.1021/la3051719 | *Langmuir* 2013, 29, 4242−4251

relies on random Brownian motion, whereas in electrophoretic deposition (EPD) an external field directs charged nanoparticles to an oppositely charged electrode. EPD has previously been used to direct colloidal nanoparticles on patterned conductive regions on surfaces but not to produce isolated nanoparticle clusters. For example, methods to design patterned nanoparticle arrays with EPD on conductive domains have been patterned either on microscale domains,[26] as isolated single nanoparticles,[27,28] or in linear domains.[27,29] In this study, a PS-*b*-PMMA thin film on highly doped Si is used as the working electrode. The film is not directly etched, but instead PMMA domains are chemically modified for chemical attachment of a thioctic acid (TA)-functionalized nanoparticle from colloid.[30] Previous studies of nanoparticle deposition with EPD have demonstrated that dielectric polymer films coated on conductive electrodes can produce nanoparticle films with homogeneous morphology of comparable quality to those deposited directly on conductive substrates.[31,32] We use aqueous-based EPD, which benefits from faster kinetics, reduced requisite voltage, suitability for materials most stable in aqueous solutions, and environmental benefits when compared to more common nonpolar solvents.[33] We find that EPD can produce comparable areal density of Au nanoparticles on PS-*b*-PMMA thin films in 1/6th of the processing time with respect to random diffusion. This is significant because processing time relates directly to processing costs. Importantly, we also find that EPD deposition leads to only a small fraction, <20%, of isolated Au nanoparticles on the surface, whereas diffusion has ∼50% isolated Au nanoparticles. Furthermore, when using EPD, Au clusters have relatively uniform interparticle spacing that is approximately 1−2 nm. We demonstrate, using electromagnetic full-wave simulations, that these two latter EPD properties lead to a 100-fold increase in electromagnetic field intensity as the interparticle spacing is decreased from 4 to 1 nm that can lead to up to a 10^4 increase in SERS intensity. These field enhancements are thus critical for decreasing detection limits in molecular sensors.

RESULTS AND DISCUSSION

First, diffusion and electrophoresis were compared in terms of Au nanoparticle coverage on the PMMA domains of PS-*b*-PMMA thin films. Figure 1a depicts how Au nanoparticles are chemically assembled on PS-*b*-PMMA thin films as described in prior work.[30] Here we show Au nanoparticles that have been functionalized with TA ligand molecules and PS-*b*-PMMA thin films that have been treated with ethylenediamine (ED) in dimethyl sulfoxide (DMSO) solution are illustrated. 1-Ethyl-3-[3-(dimethylamino)propyl]carbodiimide hydrochloride (EDC) and *N*-hydroxysulfosuccinimide (S-NHS) (EDC/S-NHS) cross-linking chemistry is then used to couple Au nanoparticles to chemically modified PMMA domains,[30] since this chemistry has been reported to induce the covalent attachment of carboxylic acid end groups with amine end groups.[34] In previous work, we have observed negligible Au nanoparticle attachment when the chemical surface treatment and cross-linking steps were not performed.[30] The diffusion deposition method is depicted in Figure 1b, where the PS-*b*-PMMA sample surface is suspended face down in the nanoparticle colloidal solution and random Brownian motion leads to surface−nanoparticle interactions. The EPD method is depicted in Figure 1c, where the PS-*b*-PMMA thin film has been deposited on highly doped Si, ρ = 0.001 ohm·cm, which is used as the working electrode. A Pt electrode is suspended in

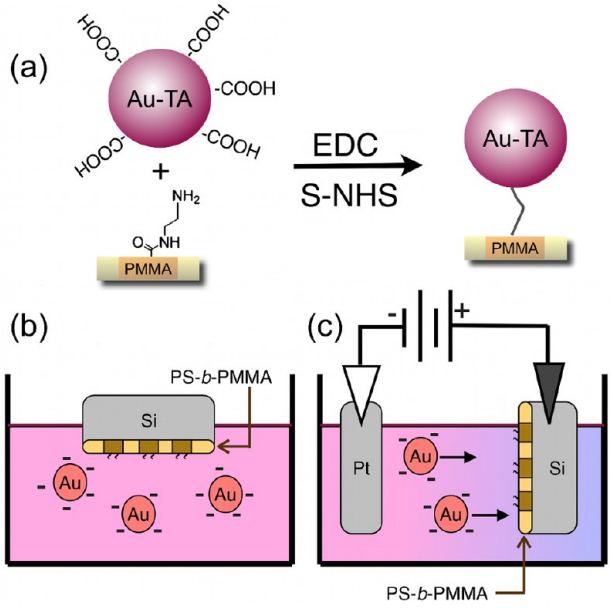

Figure 1. Illustration of chemical self-assembly of Au nanoparticles on PS-*b*-PMMA thin films showing (a) schematic of TA-functionalized Au nanoparticles with carboxylic acid end groups attached to ED-treated PMMA domains with amine end groups using EDC/S-NHS as a cross-linker. Schematics of assembly methods are shown for (b) diffusion deposition and (c) EPD.

the aqueous Au nanoparticle solution as the counter electrode. Zeta potential measurement of the TA-functionalized Au nanoparticles provides values of −52.8 ± 13.5 mV for 20 nm Au nanoparticles and −35.0 ± 5.4 mV for 10 nm Au nanoparticles, and thus the nanoparticles will be attracted to the Si sample surface with the PS-*b*-PMMA thin film with the positive applied bias. While this apparatus was designed to deposit nanoparticle clusters on a 1 cm^2 substrate, the process could theoretically be designed with larger apparatus to accommodate larger conductive substrates provided the electric field strength is maintained across the surface area of the substrate with a constant electrode distance.

PS-*b*-PMMA thin films with different surface morphology were used as templates for Au nanoparticle attachment. It is well-known that molecular weight affects the surface morphology of diblock copolymer thin films.[18,35] The molecular weights of the copolymer precursor were varied to obtain cylindrical and lamellar PMMA domains. In Figure 2, 1 μm × 1 μm AFM topography images of PS-*b*-PMMA thin films with (a) M_n of 55-*b*-22 kg mol^{-1}, referred to as b(20 nm), (b) M_n of 260-*b*-63.5 kg mol^{-1}, referred to as b(40 nm), and (c) M_n of 170-*b*-145 kg mol^{-1}, referred to as b(Lam). In Figures 2a and 2b, the observed morphology is cylindrical. PMMA domains have mean diameter of 20 nm in Figure 2a, thus are referred to as b(20 nm), and mean diameter of 40 nm in Figure 2b, thus referred to as b(40 nm). A lamellar-like configuration of PMMA domains, referred to as b(Lam), is shown in Figure 2c. Phase contrast images are included as insets in the AFM topography images of Figure 2 to clearly identify the PMMA domains that appear darker when imaged in repulsive mode during intermittent contact mode AFM imaging.[36]

To improve attachment of Au nanoparticles on PMMA domains using the EPD method, first the applied voltage during EPD was varied to maximize Au nanoparticle surface coverage using this process. Figure 3 shows SEM images of 20 nm Au

dx.doi.org/10.1021/la3051719 | *Langmuir* 2013, 29, 4242−4251

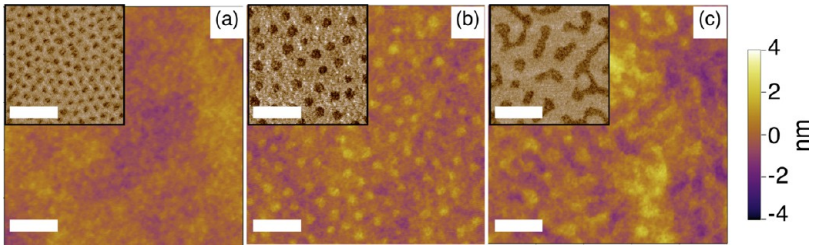

Figure 2. AFM topography images of PS-*b*-PMMA thin films with (a) M_n of 55-*b*-22 kg mol^{-1}, referred to as b(20 nm), (b) M_n of 260-*b*-63.5 kg mol^{-1}, referred to as b(40 nm), and (c) M_n of 170-*b*-145 kg mol^{-1}, referred to as b(Lam). Phase contrast AFM images are shown as insets. All scale bars are 200 nm.

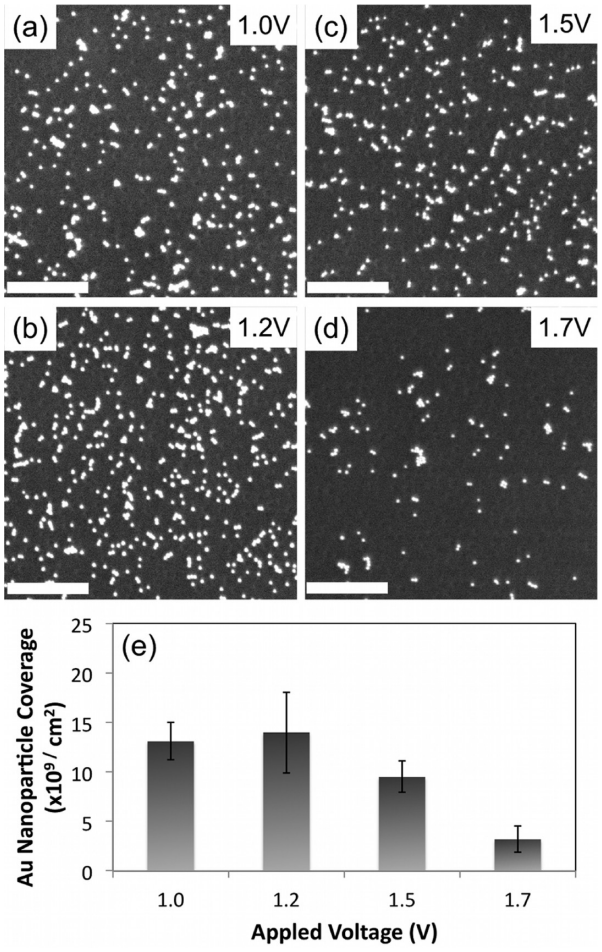

Figure 3. SEM images of 20 nm Au nanoparticles on b(40 nm) thin films after 10 min EPD at an applied voltage of (a) 1.0, (b) 1.2, (c) 1.5, and (d) 1.7 V. All scale bars are 500 nm. (e) Graph of Au nanoparticle surface coverage (average number of nanoparticles per unit area and standard deviation represented with error bars) as a function of applied EPD voltage.

nanoparticles deposited on b(40 nm) thin films using EPD for 10 min at various applied voltages: (a) 1.0, (b) 1.2, (c) 1.5, and (d) 1.7 V with a 10 mm distance between the electrodes. Figure 3e is a graph of the average Au nanoparticle surface coverage, in terms of average number of nanoparticles per unit area, for each applied voltage as determined from ten different 9 μm^2 regions on SEM images. Error bars represent the standard deviation in the measurements. The Au nanoparticle surface coverage increases with increased applied voltage up to 1.2 V and then decreases with further increases in applied voltage. The relationship between nanoparticle coverage and applied voltage observed in Figure 3 is not unexpected since the electrolysis of water will occur at voltages above 1.23 V at acidic pH and T = 25 °C based on the Nernst equation. Electrolysis will locally lower the pH near the working electrode.[37] At low pH, EDC-activated carbodiimide attachment rates will decrease and EDC decomposition will increase.[34] Other electrochemical decomposition reactions[38−40] may also occur at the electrodes. Typically reduced voltage,[27,41,42] pulsed dc fields,[37,42−44] and asymmetric ac fields[44,45] have previously been found to inhibit electrolysis. We find that voltages at or below 1.2 V appear to reduce the negative effects of water electrolysis since this yields the maximum nanoparticle surface coverage.

Diffusion deposition and EPD, with an applied voltage of 1.2 V, are directly compared for the deposition of 20 nm Au nanoparticles on b(40 nm) thin films. While increased concentration of EDC cross-linker was demonstrated in our previous work[21] to increase nanoparticle coverage and cluster formation, analysis of Au nanoparticle attachment using EPD on b(40 nm) and b(Lam) in Figure S1 of the Supporting Information demonstrated a maximum threshold of Au nanoparticle coverage without aggregation was reached after the addition of 38 μM EDC (94 μM S-NHS) and was henceforth used. In Figure 4, representative SEM images (1 μm × 1 μm) are provided of the surfaces following nanoparticle deposition by (a) diffusion for 120 min, (b) EPD for 10 min, and (c) EPD for 20 min. Larger scale 4 μm × 4 μm SEM images of the same samples are provided in the Figure S2 for the 120 min diffusion and 10 and 20 min EPD measurements. We found that without using a fresh solution no further increase of nanoparticle coverage was observed after a 60 min diffusion deposition or a 10 min EPD. The colloidal nanoparticle solutions were thus replaced with a freshly made solution every 60 min for diffusion deposition and every 10 min for EPD, since EDC has a high rate of hydrolysis during EPD. The $t_{1/2}$ of EDC is 72 min at the buffered pH of 6.2, and the hydrolysis rate increases as pH decreases.[46] Figure 4d is a graph of the average Au nanoparticle surface coverage for both diffusion deposition and EPD that was determined from SEM images of at least eight different 9−25 μm^2 regions. The data in Figure 4d demonstrate nanoparticle surface coverage increases with increased time for EPD, and after 20 min, EPD produces the same Au nanoparticle surface coverage as a 120 min diffusion process. On average, EPD produces surfaces with 28% nanoparticle coverage on PMMA domains with minimal large aggregate formation on the surface. In comparison, increases in coverage using diffusion deposition were previously achieved by increasing TA concentrations that led to some nanoparticle aggregate formation on the surface.[21]

dx.doi.org/10.1021/la3051719 | *Langmuir* 2013, 29, 4242−4251

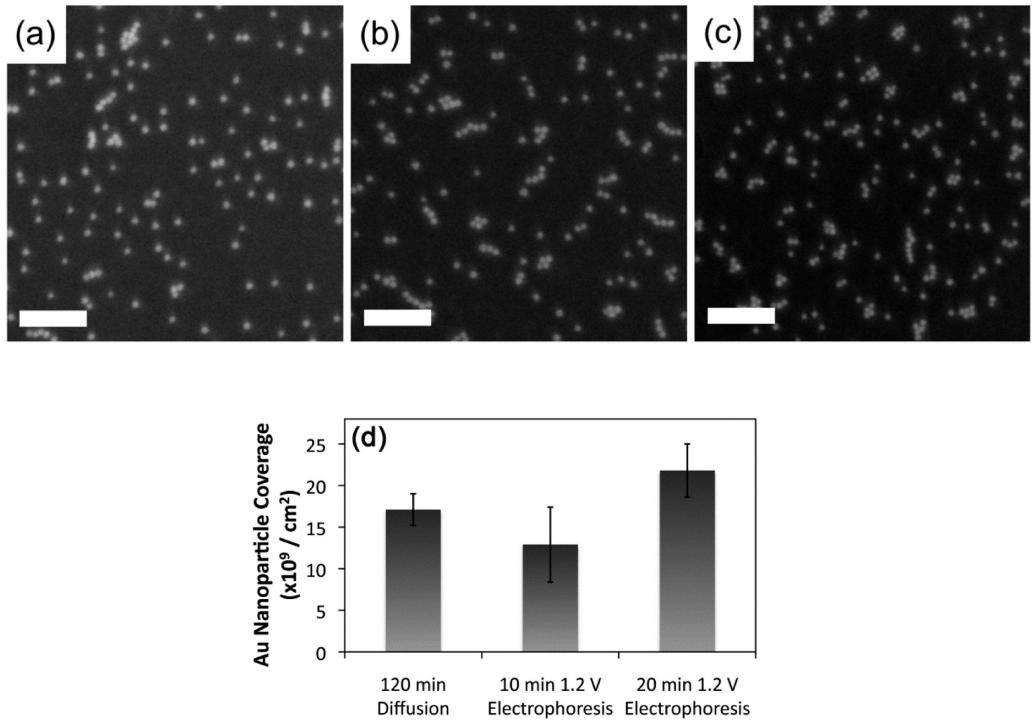

Figure 4. SEM images of 20 nm Au nanoparticles on b(40 nm) after (a) diffusion deposition for 120 min and EPD for (b) 10 or (c) 20 min. All scale bars are 200 nm. (d) Average Au nanoparticle surface coverage (average number of nanoparticles per unit area and standard deviation represented with error bars) for samples a–c acquired from at least eight different 9–25 μm^2 regions in SEM images.

One of the critical physical parameters in achieving high electric field enhancement in nanoparticle clusters is the interparticle spacing,[1,47] as it will be shown later with full-wave simulations of the local electromagnetic field, based on the finite element method. Therefore, first we show that the ED treatment of the PS-*b*-PMMA thin films and the type of deposition method, EPD versus diffusion, were both found to play a role in interparticle spacing and hence constitute important ingredients for local field enhancement. First we show how varying the ED treatment of PS-*b*-PMMA thin films affects interparticle spacing. In Figure 5, 500 nm × 500 nm AFM topography images of b(40 nm) thin films after exposure to 2 vol % ED in DMSO solution for 1 min (Figure 5a) and 5 vol % ED in DMSO for 5 min (Figure 5b) are shown. Line profiles with the same height scales are included as insets. Downward blue (green) arrows point to PMMA domains on the line profiles for the 2% (5%) ED-treated b(40 nm) thin films. Depressions of approximately 1–2 nm are observed on PMMA domains after the 2 vol % ED treatment, whereas depressions of 4–5 nm are observed for the 5 vol % ED treatment. In the latter case, elevated ridges at the edges of the PMMA domains are also observed likely due to displaced PMMA. After the 2% ED treatment and diffusion deposition, 20 and 10 nm Au nanoparticles are observed both near the center of PMMA domains and on PS/PMMA interfaces; see the SEM images of Figure 5c and 5d, respectively. Whereas after the 5% ED treatment and diffusion deposition, 20 nm (Figure 5e) and 10 nm (Figure 5f) Au nanoparticles appear to preferentially assemble at the PS/PMMA interfaces, particularly for the case of 10 nm Au nanoparticles. The preference for attachment at hydrophobic/hydrophilic interfacial, ridged features has been previously observed during diffusion[48,49] and during EPD.[29] This suggests that the Au nanoparticles attach to PS/PMMA (hydrophobic/hydrophilic)[30] interfaces

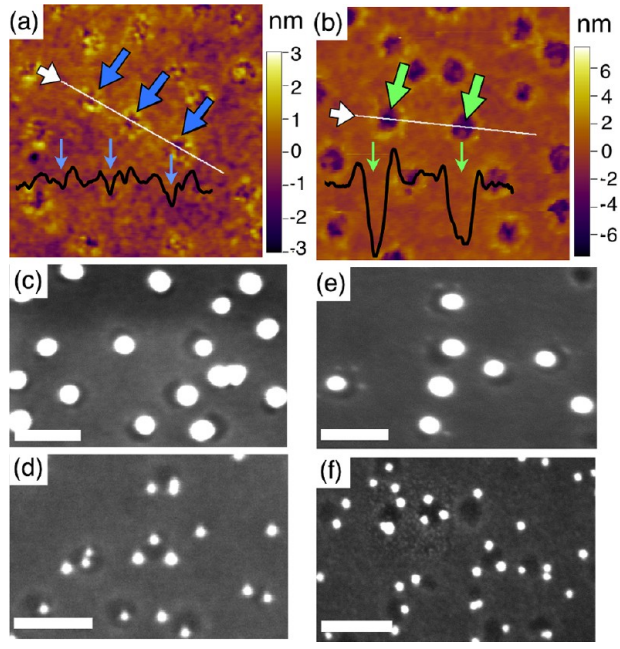

Figure 5. 500 nm × 500 nm AFM topography images of b(40 nm) thin films after exposure to (a) 2 vol % ED in DMSO solution for 1 min and (b) 5 vol % ED in DMSO solution for 5 min. Line profiles are included as insets in AFM images with the same height scale; arrows highlight the location of PMMA domains. SEM images, with 100 nm scale bars, of Au nanoparticles deposited by diffusion deposition on the (c, d) 2% and (e, f) 5% ED-treated b(40 nm) thin films. The diameter of Au nanoparticles are (c, e) 20 nm and (d, f) 10 nm.

due to the ridged surface topography due to the ED treatment. PS/PMMA interfacial ring-oriented attachment of 10 nm nanoparticles with diffusion deposition and the 5% ED

dx.doi.org/10.1021/la3051719 | *Langmuir* 2013, 29, 4242–4251

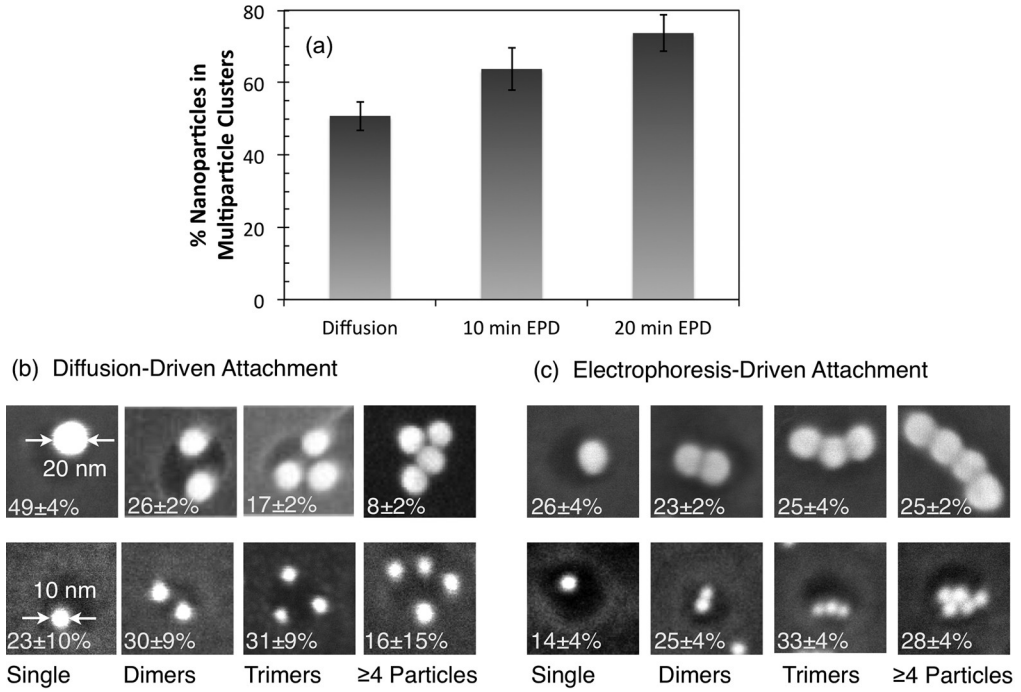

Figure 6. (a) Percentage of Au nanoparticles observed in clusters on the surface of b(40 nm) thin films as a function of deposition parameters. SEM images of Au nanoparticle clusters with diameter of 20 nm (top row) and 10 nm (bottom row) after (b) diffusion deposition and (c) EPD. The frequency of occurrence of nanopartices in each type of cluster is listed on the bottom of the SEM images.

treatment generally leads to increased interparticle spacing in clusters that is not desirable for hot spot creation but may be applicable for Fano resonances or supporting magnetic modes.[50,51]

A 5% ED treatment typically leads to higher Au nanoparticle coverage. Thus, diffusion deposition and EPD were then compared in terms of Au nanoparticle cluster formation on b(40 nm) surfaces after 5% ED treatment. In Figure 6a, the graph shows the percentage of Au nanoparticles that form multiparticle clusters on b(40 nm) thin films (the remainder are isolated Au nanoparticles) for both deposition methods. The graph was generated from SEM images, and representative images are shown in Figure S2. When comparing diffusion and EPD, the latter nearly doubles the relative number of Au nanoparticles arranged in clusters on the surface. Note that EPD on unpatterned ED-treated PMMA surfaces and SiO_2/Si surfaces did not lead to cluster formation (see Figure S3), and thus it is the combination of chemical patterning and EPD that leads to cluster formation. Figure 6b,c provides a table of approximately 80 nm × 80 nm SEM images of representative clusters on b(40) thin films observed after diffusion deposition (Figure 6b) and EPD (Figure 6c), and their frequency of occurrence is listed as text in the images. The first row of SEM images corresponds to 20 nm Au nanoparticles and the second row corresponds to 10 nm Au nanoparticles. The first, second, third, and fourth columns correspond to single particles, dimers, trimers, and larger clusters having four or more nanoparticles, respectively.

The percentage of Au nanoparticles incorporated in each type of cluster that is listed on the SEM images of Figures 6b and 6c was obtained from statistical analysis of 9 μm^2 SEM images collected at 4−8 different locations on each of the sample nanoparticle arrays. SEM analysis indicates that cluster formation during EPD has a different dynamic than during diffusion. EPD produces fewer single 20 nm Au nanoparticles, 26 ± 4%, than diffusion, which has 49 ± 4%. For both diffusion deposition and EPD methods, the PMMA domain size/nanoparticle diameter ratio was found to influence the size of the cluster. Examination of the data in Figure 6 shows that larger clusters are observed more frequently on 40 nm PMMA domains when the nanoparticle diameter was 10 nm, ratio 4/1, than when the diameter was 20 nm, ratio 2/1. Consider that after EPD deposition on b(40 nm) thin films single 10 nm Au nanoparticles on PMMA domains form with a probability of 14 ± 4% and 20 nm Au nanoparticles exist as single particles with a probability of 26 ± 4%. The number of isolated or single 10 nm particles observed decreases by at least 10% for both EPD and diffusion deposition when compared to 20 nm nanoparticles on b(40) thin films. Furthermore, when decreasing the PMMA domain size to 20 nm, the percentage of 10 nm Au nanoparticles in larger clusters, domain/diameter ratio of 2/1 (see Figure S4) is similar to 20 nm nanoparticles on 40 nm PMMA having the same ratio. Overall, the PMMA domain to nanoparticle diameter ratio influences the cluster size during diffusion deposition; larger domains yield on average larger clusters when the nanoparticle diameter is fixed.

An increase in dimers and trimers on the surface is important since these types of clusters are associated with high electric field enhancements as shown in simulations in our previous studies.[21] Furthermore, when using EPD, the average interparticle spacing in clusters decreased to approximately 1−2 nm and is more uniform in comparison to diffusion deposition when examining the SEM images of Figure 6. Examination of the same Figure 6 shows that the interparticle gap spacing for 20 nm Au nanoparticles in clusters was 2−7 nm on average with diffusion deposition. Uniformity of interparticle spacing with isolated nanoparticle clusters has been quite challenging using self-assembly methods, generally requiring the addition of a molecular cross-linker between the nanoparticles.[52] The reduced interparticle spacing observed after

dx.doi.org/10.1021/la3051719 | *Langmuir* 2013, 29, 4242−4251

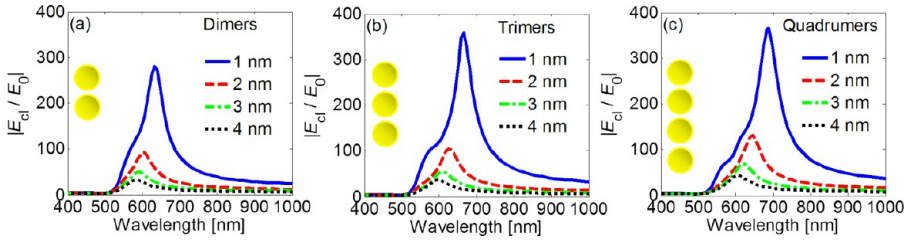

Figure 7. Theoretical electric field enhancement $|E_{cl}/E_0|$ computed in dimers, linear trimers, and linear quadrumers versus illumination wavelength when excited with a plane wave orthogonal to the surface, with electric field polarized along the cluster axis. Results retrieved via full-wave simulations employing the finite element method for various gap sizes.

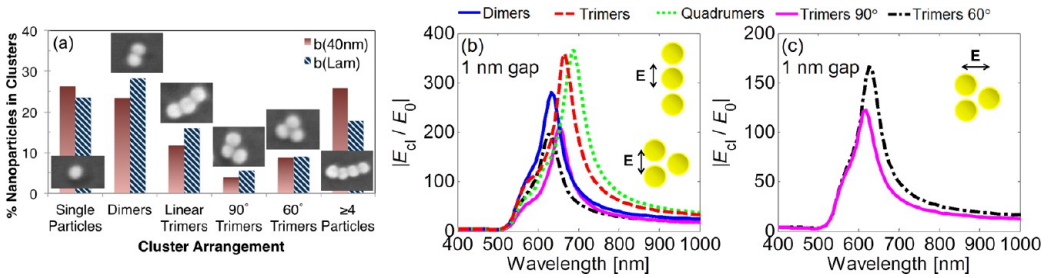

Figure 8. (a) Percentage of Au nanoparticles observed in single particle clusters, dimers, linear trimers, 90° trimers, 60° trimers, and larger clusters on b(40 nm) and b(Lam) thin films using EPD acquired from SEM data. (b, c) Electric field enhancement for the two polarizations of the incident plane wave in the insets for various cluster configurations: dimers, linear trimers, trimers 60°, trimers 90°, and linear quadrumers, for a gap of 1 nm between nanoparticles. The linear configurations are not reported in (c) because the wave is not expected to couple for plane wave polarization orthogonal to the cluster axis.

EPD may be associated with intertwining of the ligand (for thioctic acid it is ∼1 nm in length).[41] Derjaguin−Laudau−Verwey−Overbeck (DLVO) theory also predicts that the double layer thins near the electrode surface due to increased in ionic strength;[53] in this case van der Waals forces will also lead to smaller interparticle spacings.[54,55] The decrease in interparticle spacing with EPD is critically important for local electric field enhancements that are expected to rapidly increase with decreasing interparticle spacing as this value goes below 10 nm.[56]

Using our previous setup,[21] we performed full-wave simulations employing the finite element method (high frequency structure simulator, HFSS, by Ansys Inc.) in order to investigate the effect of changing interparticle gap spacing on SERS enhancement. In Figure 7, calculated electric field enhancements for 1−4 nm gap spacings between nanoparticles in representative cluster configurations observed in SEM images of Figure 6 are shown. We consider dimers, linear trimers, and linear quadrumers since these represent dominant nanoparticle configurations observed on fabricated samples. The electric field enhancement is here intended as $|E_{cl}/E_0|$, where E_0 is the plane wave field without clusters (still accounting for the multilayered environment in simulations as discussed next) and E_{cl} is the field with clusters, occurring between the nanoparticles in the middle of the gap between contiguous nanoparticles. Therefore, we investigate the field enhancement in the "hot spots". Moreover, Au nanoparticles have diameter of ≈20 nm with permittivity taken from ref 57 and have been assumed to be embedded in a layer with dielectric constant of 2.47 (40 nm thickness) on top of a silicon substrate. This dielectric permittivity of 2.47 is close in value to the one of PMMA and a layer of benzenethiol molecules covering the nanoparticles (in the simulations the nanoparticles are assumed to be at the center of the 40 nm thick layer). For simplicity of calculations we array the clusters in a square lattice, with a period large enough to affect weakly the maximum field between the nanoparticles in a cluster (see Supporting Information in ref 21) so as the clusters can be considered isolated. We illuminate each cluster configuration with a plane wave, with incidence orthogonal to the surface, with electric field polarized along the axis of the linear cluster, for the range of excitation wavelengths between 400 and 1000 nm. Results in Figure 7 show that a slight increase in the gap size dramatically diminishes the local electric field enhancement, going for example from about ≈365 for the linear quadrumer case with 1 nm gap to about ≈130 when the gap is 2 nm to values less than ≈45 when the gap is 4 nm. We note also the resonance blue shift for increasing gap size. Calculation of the local electric field enhancement allows us to infer an estimate of the theoretical SERS enhancement, simply computed here as the fourth power of the field enhancement $|E_{cl}/E_0|^4$, which would range from about $\approx 10^{10}$ for the linear quadrumer case with 1 nm gap to about $\approx 3 \times 10^8$ when the gap is 2 nm and finally to values less than $\approx 4 \times 10^6$ when the gap is 4 nm. This shows the potential of substrates made of linear and triangular clusters of closely spaced nanoparticles for SERS applications. Since EDP enables a higher fraction of clusters with smaller gap size, it is expected that this method will lead to improved performance for sensing applications.

Polymer surface morphology was varied to examine the effects on Au nanoparticle assembly. Au nanoparticle attachment on b(Lam), which has 48% PMMA surface area was compared to that on b(40 nm), which has 20% PMMA surface area. Analysis of the SEM images, shown in Figure S1, demonstrates that Au surface coverage is ∼10% higher on b(Lam) surfaces. Figure 8a summarizes SEM data analyses and shows the percentage of nanoparticle assemblies in each of the listed clusters. Note the increased number of dimer and linear trimer cluster arrangements with b(Lam) when compared with b(40 nm). Using the same setup described to compute the

dx.doi.org/10.1021/la3051719 | Langmuir 2013, 29, 4242−4251

results shown in Figure 7, we report in Figure 8b,c full-wave electromagnetic results showing the theoretical electric field enhancement $|E_{cl}/E_0|$ for different cluster configurations. In the case of triangular trimers, SEM images show that nanoparticles may be clustered with various angular values. That is why we analyze here two representative cases of 60° and 90° angles. Interparticle gap size is kept equal to 1 nm, as in the previous case for linear clusters, as well of the triangular clusters now considered. We illuminate each structure with a plane wave, with incidence orthogonal to the surface, with electric field polarized along the two directions in Figure 8b,c for the range of excitation wavelengths between 400 and 1000 nm. Results in Figure 8b,c show that stronger electric field enhancement is achieved with linear clusters (dimers, trimers, quadrumers) around 650 nm with respect to other trimer (triangular) configurations. We observe both increasing electric field enhancement and a resonance red shift for increasing number of particles in the linear configurations. We also note that electric field enhancement values, relative to the gap distances here considered, are not very sensitive to the angular value in triangular trimers. Furthermore, for these clusters, one polarization of the incident plane wave leads to slightly stronger electric field enhancement with respect to the other. These simulations overall show that the increased number of dimers and trimers arrangements is important for use in sensing applications. Linear trimers and quadrumers provide stronger electric field enhancement than triangular clusters, when the polarization matches with the axis of the linear cluster. Vice versa, triangular clusters provide slightly weaker fields than linear trimers and quadrumers, but their field enhancement, and thus SERS, is robust with respect to the polarization. Indeed, we estimate SERS enhancements of about 10^9–10^{10} when computed as the fourth power of the field enhancement. As a consequence of such numerical results, we estimate that EPD attachment on b(Lam) PS-*b*-PMMA array provides a SERS surface that produces stronger signal enhancements as compared to b(40 nm) due to the combination of both increased total nanoparticle attachment and increased frequency of nanoparticle clustering in such configurations.

CONCLUSIONS

In this study, we compare EPD to diffusion deposition for assembly of Au nanoparticle clusters on PMMA domains of PS-*b*-PMMA thin films. We find that EPD, when adjusting dc voltage to reduce electrolysis, requires only 1/6th the processing time as diffusion for achieving comparable Au nanoparticle surface coverage, $>10^{10}$ nanoparticles/cm^2. EPD leads to more Au nanoparticles forming clusters on the surface versus diffusion assembly for both 10 and 20 nm diameter nanoparticles. The plasmon resonance of 20 nm Au nanoparticles, as determined from full wave simulations, occurs near the wavelength of a helium–neon laser (633 nm) and thus can be excited with a standard laser. Optimization of the EPD process using an ac field,[44,45] for example, could be used to increase Au coverage in future work while still keeping the coverage below the hexagonally close packed limit where electric field enhancements decrease.[21] Moreover, EPD demonstrated more uniformity of the interparticle spacing within nanoparticle clusters, with average spacing of 1–2 nm for EPD in comparison to 2–7 nm for diffusion deposition. The decreased interparticle spacing within clusters is important for achieving increased electric field enhancements as demonstrated by electromagnetic full-wave simulations. Simulations demonstrated that dimer, linear trimer, and linear quadrumer nanoparticle clusters produced the strongest enhancements when comparing enhancements in isolated clusters considered here. When the interparticle spacing in the clusters is reduced to 1 nm, we estimate an increase in the local electric field enhancement. When estimating a theoretical SERS enhancement (defined as the fourth power of the electric field enhancement in the hot spots), we find the SERS enhancement can reach values as large as 10^{10} for the linear cluster configurations. In the case of triangular trimer configurations, we estimate slightly lower field enhancements than linear clusters; the theoretical SERS enhancements is estimated to reach $\sim 10^9$ when the interparticle spacing is 1 nm, and SERS is not expected to be strongly dependent on the polarization. PS-*b*-PMMA surface morphology affected cluster formation; on lamellar-like surface morphologies, b(Lam), we observe an increased frequency of the more strongly field enhancing dimers and linear trimers in SEM images as compared to cylindrical PMMA configurations, b(40 nm). Because of the higher coverage of PMMA domains on b(Lam) versus b(40 nm), we also obtain a higher overall coverage of Au nanoparticles on the surface. Optimization of b(Lam) surfaces in terms of uniformity of PMMA domains and EPD deposition parameters would be a good starting point for optimizing sensor performance. Overall, EPD produces a distribution of clusters on the surface that include a high coverage of dimers, trimers, and quadrumers with nanometer interparticle gap spacings that are calculated to exhibit high electric field enhancements. EPD thus represents a low-cost method that is highly desirable for the development of molecular scale sensors.

MATERIALS AND METHODS

Materials. The random copolymer poly(styrene-*co*-methyl methacrylate)-*α*-hydroxyl-*ω*-tempo moiety (PS-*r*-PMMA) (M_n = 7400, 59.6% PS) and block copolymer poly(styrene-*b*-methyl methacrylate) (PS-*b*-PMMA) (of molecular weights b(20 nm) M_n = 55-*b*-22 kg mol^{-1}, b(40 nm) M_n = 260-*b*-63.5 kg mol^{-1}, and b(Lam) M_n = 170-*b*-144 kg mol^{-1}) were purchased from Polymer Source, Inc. (Dorval, Canada). Boron-doped silicon wafers with of resistivity 1–10 ohm·cm for diffusion deposition were purchased from University Wafer (South Boston, MA), and Si wafers with resistivity of 0.001–0.004 ohm·cm for electrophoresis deposition (EPD) were purchased from Virginia Semiconductor (Frederickburg, VA). Gold(III) chloride trihydrate ($HAuCl_4{\cdot}3H_2O$), DL-6,8-thioctic acid ($C_8H_{14}O_2S1$) (TA), ethylenediamine (ED), dimethyl sulfoxide (DMSO), ethanol, isopropanol (IPA), toluene, and 52 mesh Pt gauze foil were purchased from Sigma-Aldrich (St. Louis, MO). 10 nm diameter unconjugated Au nanoparticle aqueous colloid (British Biocell Intl.) and 20 nm diameter citrate-capped Ag nanoparticle colloid (PELCO NanoXact) were purchased from Ted Pella (Redding, CA). Sodium citrate, sodium hydroxide (NaOH), and hydrofluoric acid (HF) were purchased from Fisher Scientific (Pittsburgh, PA). 2-(*N*-morpholino)ethanesulfonic acid (MES) 0.1 M buffer, 1-ethyl-3-[3-(dimethylamino)propyl]-carbodiimide hydrochloride (EDC), and *N*-hydroxysulfosuccinimide (S-NHS) were purchased from Pierce (Rockford, IL). Nanopure deionized water (DI) (18.2 MΩ cm^{-1}) was obtained from a Milli-Q Millipore system and used for all experiments.

Diblock Copolymer Thin Film Preparation and Chemical Functionalization. Solutions of 1 wt % PS-*r*-PMMA random copolymer, with anchoring *α*-hydroxy-*ω*-tempo moiety end groups, in toluene are deposited by spin-coating at 3000 rpm for 45 s on Si substrates. Si substrates were cleaned with 10% v/v HF/DI and treated with a fresh oxide layer by rinsing with DI. PS-*r*-PMMA films were annealed at 170 °C for 72 h in vacuum and rinsed with toluene after to form a brush layer of 6–7 nm PS-*r*-PMMA with ∼59.6% surface coverage of PS. The PS-*b*-PMMA thin film layer was deposited by

dx.doi.org/10.1021/la3051719 | Langmuir 2013, 29, 4242–4251

spin-coating at 5000 rpm for 45 on the random copolymer brush an annealing at 170 °C. Annealing continued for 72 h for the b(20 nm) and b(Lam) and 120 h for the b(40 nm) configuration. The PS-*b*-PMMA substrates were rinsed with 50/50 v/v IPA/DI for 1 min followed by immersion in DMSO for 5 min and 1−5 min immersion in 2−5% vol % ED in DMSO to functionalize the surface PMMA regions of the substrate with amine functional groups.[58] The standard treatment of ED was for 5 min in 5 vol % ED in DMSO solution. Any deviations are clearly stated in the text. The surfaces were rinsed with IPA after ED treatment.

Au Nanoparticle Synthesis and Functionalization. Au nanoparticles with 20 nm diameter were synthesized by citrate reduction of 0.01 wt % $HAuCl_4 \cdot 3H_2O$ in aqueous sodium citrate solution using the Turkevich method.[59] The 20 nm Au nanoparticles were functionalized with TA at concentration 0.50 mM by the addition of 10 μL of 0.05 M TA ethanolic solution for each milliliter of Au nanoparticle solution readjusted to pH 11.67 with dilute NaOH, followed by 18 h continuous stirring. Citrate stabilized colloidal Au nanoparticles of 10 nm diameter (and colloidal Ag nanoparticles of 20 nm diameter) were purchased in 0.01 wt % aqueous solution to maintain consistent particle size. This Au nanoparticle solution was functionalized with TA after replacing the solvent with pH 11.67 dilute NaOH solution as previously reported in Choi et al.[30] The 10 nm Au nanoparticles were functionalized with TA at concentration 0.25 mM. For both types of nanoparticles, the residual TA was removed from the nanoparticle solution and the basicity reduced to pH 8 by centrifuging at 7000*g* for 20 min for 20 nm Au nanoparticles and 65000*g* for 50 min for 10 nm Au nanoparticles. This was followed by resuspension in DI water at twice the nanoparticle concentration for the 20 nm nanoparticles and at the same nanoparticle concentration for the 10 nm nanoparticles.

Introduction of Chemical Cross-Linker. The chemical cross-linker EDC/S-NHS was introduced to the aqueous colloidal TA-functionalized Au nanoparticle solution at concentrations ranging from 20 to 52 μM EDC from 2 mM EDC in 0.1 M MES buffer and 50−130 μM S-NHS from 5 mM S-NHS in 0.1 M MES buffer with a molar ratio of 0.4:1.0 EDC:S-NHS maintained. The standard concentrations of EDC:S-NHS were prepared at 38:95 μM for 20 nm Au nanoparticles and at 20:50 μM for 10 nm Au nanoparticles. Any deviations are clearly stated in the text.

Chemical Cross-Linking Attachment by the Diffusion Deposition Method. The ED-treated PS-*b*-PMMA thin films on Si were horizontally suspended in 2 mL of the cross-linker-activated Au nanoparticle solution for each cm^2 of substrate with the functionalized side of the PS-*b*-PMMA thin film immersed facedown and incubated at 40 °C for 120 min (in 60 min durations with refreshed nanoparticle solution) followed by IPA wash.

Chemical Cross-Linking Attachment by the EPD Method. The ED-treated PS-*b*-PMMA thin films on Si (anode) were vertically suspended parallel to a Pt mesh electrode (cathode) with 10 mm separation in a 10 mL beaker and connected to a BK Precision 1621a dc-regulated power supply. Both the PS-*b*-PMMA thin films on Si and the Pt electrode were immersed in 4 mL of the cross-linker-activated Au nanoparticle solution, and a constant voltage of up to 1.7 V for 10−20 min was applied (in 10 min durations with refreshed nanoparticle solution). The standard EPD voltage used was 1.2 V. Any deviations are clearly stated in the text. Afterward, the samples were rinsed with IPA.

Nanocharacterization. The surfaces were analyzed with atomic force microscopy (AFM) using an Asylum Research MFP 3D AFM (Santa Barbara, CA) with 75 kHz resonance frequency probes with diamond-like carbon coating produced by BudgetSensors. Scanning electron microscopy (SEM) analysis was measured with a Sirion XL30 SFEG (FEI, Hillsboro, OR), a Quanta3D Dual Beam SEM (FEI), and a Magellan XHR SEM (FEI).

■ ASSOCIATED CONTENT

Supporting Information

Additional figures as described in the text, SEM images of the effects of varying EDC concentration with EPD of Au nanoparticles on b(20 nm) and b(Lam) (Figure S1), 4 μm × 4 μm SEM images of samples from Figure 4 (Figure S1), SEM images of Au nanoparticle attachment by EPD on PMMA thin film on Si and SiO_2/Si substrates (Figure S2), and SEM image of 10 nm Au nanoparticles on b(20 nm) deposited by EPD on b(20 nm) with nanoparticle cluster frequency analysis (Figure S3). This material is available free of charge via the Internet at http://pubs.acs.org.

■ AUTHOR INFORMATION

Corresponding Author

*E-mail: rragan@uci.edu.

Notes

The authors declare no competing financial interest.

■ ACKNOWLEDGMENTS

The authors acknowledge the National Science Foundation CHE-0748912 and CMMI-1101074 for funding this work. The authors also acknowledge the use of the facilities within the Laboratory for Electron and X-ray Instrumentation (LEXI) at the University of California, Irvine. The authors also thank Ansys Inc. for providing HFSS that was instrumental in this work.

■ ABBREVIATIONS

SERS, surface-enhanced Raman scattering; EPD, electrophoretic deposition; PS, polystyrene; PMMA, poly(methyl methacrylate); *-b-*, *-block-*; TA, DL-6,8-thioctic acid; b(20 nm), 20 nm PMMA diameter cylindrical PS-*b*-PMMA diblock copolymer; b(40 nm), 40 nm PMMA diameter cylindrical PS-*b*-PMMA diblock copolymer; b(Lam), lamellar PS-*b*-PMMA diblock copolymer; ED, ethylenediamine; DMSO, dimethyl sulfoxide; IPA, isopropanol; NaOH, sodium hydroxide; HF, hydrofluoric acid; MES, 2-(*N*-morpholino)-ethanesulfonic acid; EDC, 1-ethyl-3-[3-(dimethylamino)-propyl]carbodiimide hydrochloride; S-NHS, *N*-hydroxysulfosuccinimide; DI, deionized water; AFM, atomic force microscopy; SEM, scanning electron microscopy; DLVO, Derjaguin−Laudau−Verwey−Overbeck.

■ REFERENCES

(1) Su, K. H.; Wei, Q. H.; Zhang, X.; Mock, J. J.; Smith, D. R.; Schultz, S. Interparticle Coupling Effects on Plasmon Resonances of Nanogold Particles. *Nano Lett.* **2003**, *3* (8), 1087−1090.

(2) Nordlander, P.; Oubre, C.; Prodan, E.; Li, K.; Stockman, M. I. Plasmon Hybridization in Nanoparticle Dimers. *Nano Lett.* **2004**, *4* (5), 899−903.

(3) Roy, S.; Dixit, C. K.; Woolley, R.; O'Kennedy, R.; McDonagh, C. Synthesis and Characterization of a Noble Metal Enhanced Optical Nanohybrid (NEON): A High Brightness Detection Platform Based on a Dye-Doped Silica Nanoparticle. *Langmuir* **2012**, *28* (21), 8244−8250.

(4) Grubisic, A.; Ringe, E.; Cobley, C. M.; Xia, Y.; Marks, L. D.; Van Duyne, R. P.; Nesbitt, D. J. Plasmonic Near-Electric Field Enhancement Effects in Ultrafast Photoelectron Emission: Correlated Spatial and Laser Polarization Microscopy Studies of Individual Ag Nanocubes. *Nano Lett.* **2012**, *12* (9), 4823−4829.

(5) Zhang, Q.; Li, N.; Goebl, J.; Lu, Z.; Yin, Y. A Systematic Study of the Synthesis of Silver Nanoplates: Is Citrate a "Magic" Reagent? *J. Am. Chem. Soc.* **2011**, *133* (46), 18931−18939.

(6) Knight, M. W.; Liu, L.; Wang, Y.; Brown, L.; Mukherjee, S.; King, N. S.; Everitt, H. O.; Nordlander, P.; Halas, N. J. Aluminum Plasmonic Nanoantennas. *Nano Lett.* **2012**, *12* (11), 6000−6004.

(7) Prodan, E.; Nordlander, P.; Halas, N. J. Electronic Structure and Optical Properties of Gold Nanoshells. *Nano Lett.* **2003**, *3* (10), 1411−1415.
(8) Myroshnychenko, V.; Rodriguez-Fernandez, J.; Pastoriza-Santos, I.; Funston, A. M.; Novo, C.; Mulvaney, P.; Liz-Marzan, L. M.; Garcia de Abajo, F. J. Modelling the Optical Response of Gold Nanoparticles. *Chem. Soc. Rev.* **2008**, *37* (9), 1792−1805.
(9) Vallecchi, A.; Campione, S.; Capolino, F. Symmetric and Antisymmetric Resonances in a Pair of Metal-Dielectric Nanoshells: Tunability and Closed-Form Formulas. *J. Nanophotonics* **2010**, *4* (1), 041577−041577.
(10) Vallecchi, A.; Albani, M.; Capolino, F. Collective Electric and Magnetic Plasmonic Resonances in Spherical Nanoclusters. *Opt. Express* **2011**, *19* (3), 2754−2772.
(11) García-Martín, A.; Ward, D. R.; Natelson, D.; Cuevas, J. C. Field Enhancement in Subnanometer Metallic Gaps. *Phys. Rev. B* **2011**, *83* (19), 193404.
(12) Aubry, A.; Lei, D. Y.; Maier, S. A.; Pendry, J. B. Interaction between Plasmonic Nanoparticles Revisited with Transformation Optics. *Phys. Rev. Lett.* **2010**, *105* (23), 233901.
(13) Cord, B.; Yang, J.; Duan, H.; Joy, D. C.; Klingfus, J.; Berggren, K. K. In *Limiting Factors in Sub-10 nm Scanning-Electron-Beam Lithography*; AVS: New York, 2009; pp 2616−2621.
(14) Gao, B.; Arya, G.; Tao, A. R. Self-Orienting Nanocubes for the Assembly of Plasmonic Nanojunctions. *Nat. Nanotechnol.* **2012**, *7* (7), 433−437.
(15) Stuen, K. O.; Detcheverry, F. A.; Craig, G. S. W.; Thomas, C. S.; Farrell, R. A.; Morris, M. A.; Pablo, J. J. d.; Nealey, P. F. Graphoepitaxial Assembly of Asymmetric Ternary Blends of Block Copolymers and Homopolymers. *Nanotechnology* **2010**, *21* (49), 495301.
(16) Liu, C.-C.; Han, E.; Onses, M. S.; Thode, C. J.; Ji, S.; Gopalan, P.; Nealey, P. F. Fabrication of Lithographically Defined Chemically Patterned Polymer Brushes and Mats. *Macromolecules* **2011**, *44* (7), 1876−1885.
(17) Xu, T.; Kim, H.-C.; DeRouchey, J.; Seney, C.; Levesque, C.; Martin, P.; Stafford, C. M.; Russell, T. P. The Influence of Molecular Weight on Nanoporous Polymer Films. *Polymer* **2001**, *42* (21), 9091−9095.
(18) Guarini, K. W.; Black, C. T.; Yeuing, S. H. I. Optimization of Diblock Copolymer Thin Film Self Assembly. *Adv. Mater.* **2002**, *14* (18), 1290−1294.
(19) Stoykovich, M. P.; Muller, M.; Kim, S. O.; Solak, H. H.; Edwards, E. W.; de Pablo, J. J.; Nealey, P. F. Directed Assembly of Block Copolymer Blends into Nonregular Device-Oriented Structures. *Science* **2005**, *308* (5727), 1442−1446.
(20) Kim, S. H.; Misner, M. J.; Xu, T.; Kimura, M.; Russell, T. P. Highly Oriented and Ordered Arrays from Block Copolymers via Solvent Evaporation. *Adv. Mater.* **2004**, *16* (3), 226−231.
(21) Adams, S. M.; Campione, S.; Caldwell, J. D.; Bezares, F. J.; Culbertson, J. C.; Capolino, F.; Ragan, R. Non-lithographic SERS Substrates: Tailoring Surface Chemistry for Au Nanoparticle Cluster Assembly. *Small* **2012**, *8* (14), 2239−2249.
(22) Moskovits, M.; Jeong, D. H. Engineering Nanostructures for Giant Optical Fields. *Chem. Phys. Lett.* **2004**, *397* (1−3), 91−95.
(23) Yan, B.; Thubagere, A.; Premasiri, W. R.; Ziegler, L. D.; Dal Negro, L.; Reinhard, B. r. M. Engineered SERS Substrates with Multiscale Signal Enhancement: Nanoparticle Cluster Arrays. *ACS Nano* **2009**, *3* (5), 1190−1202.
(24) Pillai, S.; Catchpole, K. R.; Trupke, T.; Green, M. A. Surface Plasmon Enhanced Silicon Solar Cells. *J. Appl. Phys.* **2007**, *101* (9), 093105.
(25) Schaadt, D. M.; Feng, B.; Yu, E. T. Enhanced Semiconductor Optical Absorption via Surface Plasmon Excitation in Metal Nanoparticles. *Appl. Phys. Lett.* **2005**, *86* (6), 063106.
(26) Choi, W. M.; Park, O. O. The Fabrication of Micropatterns of a 2D Colloidal Assembly by Electrophoretic Deposition. *Nanotechnology* **2006**, *17* (1), 325.
(27) Zhang, Q.; Xu, T.; Butterfield, D.; Misner, M. J.; Ryu, D. Y.; Emrick, T.; Russell, T. P. Controlled Placement of CdSe Nanoparticles in Diblock Copolymer Templates by Electrophoretic Deposition. *Nano Lett.* **2005**, *5* (2), 357−361.
(28) Patel, M. N.; Williams, R. D.; May, R. A.; Uchida, H.; Stevenson, K. J.; Johnston, K. P. Electrophoretic Deposition of Au Nanocrystals inside Perpendicular Mesochannels of TiO_2. *Chem. Mater.* **2008**, *20* (19), 6029−6040.
(29) Xiong, X.; Makaram, P.; Busnaina, A.; Bakhtari, K.; Somu, S.; McGruer, N.; Park, J. Large Scale Directed Assembly of Nanoparticles Using Nanotrench Templates. *Appl. Phys. Lett.* **2006**, *89* (19), 193108−3.
(30) Choi, J. H.; Adams, S. M.; Ragan, R. Design of a Versatile Chemical Assembly Method for Patterning Colloidal Nanoparticles. *Nanotechnology* **2009**, *20* (6), 065301.
(31) Hasan, S. A.; Kavich, D. W.; Mahajan, S. V.; Dickerson, J. H. Electrophoretic Deposition of CdSe Nanocrystal Films onto Dielectric Polymer Thin Films. *Thin Solid Films* **2009**, *517* (8), 2665−2669.
(32) Hasan, S. A.; Kavich, D. W.; Dickerson, J. H. Sacrificial Layer Electrophoretic Deposition of Free-Standing Multilayered Nanoparticle Films. *Chem. Commun.* **2009**, *25*, 3723−3725.
(33) Tang, F.; Uchikoshi, T.; Ozawa, K.; Sakka, Y. Electrophoretic Deposition of Aqueous Nano-γ-Al_2O_3 Suspensions. *Mater. Res. Bull.* **2002**, *37* (4), 653−660.
(34) Grabarek, Z.; Gergely, J. Zero-Length Crosslinking Procedure with the Use of Active Esters. *Anal. Biochem.* **1990**, *185* (1), 131−135.
(35) Matsen, M. W.; Bates, F. S. Unifying Weak- and Strong-Segregation Block Copolymer Theories. *Macromolecules* **1996**, *29* (4), 1091−1098.
(36) Krausch, G.; Hipp, M.; Boeltau, M.; Marti, O.; Mlynek, J. High-Resolution Imaging of Polymer Surfaces with Chemical Sensitivity. *Macromolecules* **1995**, *28* (1), 260−263.
(37) Besra, L.; Uchikoshi, T.; Suzuki, T. S.; Sakka, Y. Experimental Verification of pH Localization Mechanism of Particle Consolidation at the Electrode/Solution Interface and Its Application to Pulsed DC Electrophoretic Deposition (EPD). *J. Eur. Ceram. Soc.* **2010**, *30* (5), 1187−1193.
(38) Besra, L.; Liu, M. A Review on Fundamentals and Applications of Electrophoretic Deposition (EPD). *Prog. Mater. Sci.* **2007**, *52* (1), 1−61.
(39) Moreno, R.; Ferrari, B. Effect of the Slurry Properties on the Homogeneity of Alumina Deposits Obtained by Aqueous Electrophoretic Deposition. *Mater. Res. Bull.* **2000**, *35* (6), 887−897.
(40) Ferrari, B.; Moreno, R. Zirconia Thick Films Deposited on Nickel by Aqueous Electrophoretic Deposition. *J. Electrochem. Soc.* **2000**, *147* (8), 2987−2992.
(41) Kooij, E. S.; Brouwer, E. A. M.; Poelsema, B. Electric Field Assisted Nanocolloidal Gold Deposition. *J. Electroanal. Soc.* **2007**, *611* (1−2), 208−216.
(42) Zhao, S. Y.; Lei, S. B.; Chen, S. H.; Ma, H. Y.; Wang, S. Y. Assembly of Two-Dimensional Ordered Monolayers of Nanoparticles by Electrophoretic Deposition. *Colloid Polym. Sci.* **2000**, *278* (7), 682−686.
(43) Xu, Y. Z.; Zhang, Y. R.; Zheng, J. F.; Guo, C.; Niu, Z. J.; Li, Z. L. Assembly of Aggregated Colloidal Gold Nanoparticles on Gold Electrodes by In Situ Produced H^+ Ions for SERS Substrates. *Int. J. Electrochem. Sci.* **2011**, *6* (3), 664−672.
(44) Chávez-Valdez, A.; Boccaccini, A. R. Innovations in Electrophoretic Deposition: Alternating Current and Pulsed Direct Current Methods. *Electrochim. Acta* **2012**, *65* (0), 70−89.
(45) Neirinck, B.; Fransaer, J.; Biest, O. V. d.; Vleugels, J. Aqueous Electrophoretic Deposition in Asymmetric AC Electric Fields (AC−EPD). *Electrochem. Commun.* **2009**, *11* (1), 57−60.
(46) Paula Lei, Q.; Lamb, D. H.; Heller, R. K.; Shannon, A. G.; Ryall, R.; Cash, P. Kinetic Studies on the Rate of Hydrolysis of N-ethyl-N2-(dimethylaminopropyl)carbodiimide in Aqueous Solutions Using Mass Spectrometry and Capillary Electrophoresis. *Anal. Biochem.* **2002**, *310* (1), 122−124.

(47) Sweatlock, L. A.; Maier, S. A.; Atwater, H. A.; Penninkhof, J. J.; Polman, A. Highly Confined Electromagnetic Fields in Arrays of Strongly Coupled Ag Nanoparticles. *Phys. Rev. B* **2005**, *71* (23), 235408.
(48) Cui, Y.; Björk, M. T.; Liddle, J. A.; Sönnichsen, C.; Boussert, B.; Alivisatos, A. P. Integration of Colloidal Nanocrystals into Lithographically Patterned Devices. *Nano Lett.* **2004**, *4* (6), 1093−1098.
(49) Su, G.; Guo, Q.; Palmer, R. E. Colloidal Lines and Strings. *Langmuir* **2003**, *19* (23), 9669−9671.
(50) Luk'yanchuk, B.; Zheludev, N. I.; Maier, S. A.; Halas, N. J.; Nordlander, P.; Giessen, H.; Chong, C. T. The Fano Resonance in Plasmonic Nanostructures and Metamaterials. *Nat. Mater.* **2010**, *9* (9), 707−715.
(51) Sheikholeslami, S. N.; García-Etxarri, A.; Dionne, J. A. Controlling the Interplay of Electric and Magnetic Modes via Fano-like Plasmon Resonances. *Nano Lett.* **2011**, *11* (9), 3927−3934.
(52) Carroll, J. B.; Frankamp, B. L.; Rotello, V. M. Self-Assembly of Gold Nanoparticles through Tandem Hydrogen Bonding and Polyoligosilsequioxane (POSS)-POSS Recognition Processes. *Chem. Commun.* **2002**, *17*, 1892−1893.
(53) Sarkar, P.; Nicholson, P. S. Electrophoretic Deposition (EPD): Mechanisms, Kinetics, and Application to Ceramics. *J. Am. Ceram. Soc.* **1996**, *79* (8), 1987−2002.
(54) Hamaker, H. C. Formation of a Deposit by Electrophoresis. *Trans. Faraday Soc.* **1940**, *35*, 279−287.
(55) Hamaker, H. C.; Verwey, E. J. W. Part II. (C) Colloid Stability. The Role of the Forces between the Particles in Electrodeposition and Other Phenomena. *Trans. Faraday Soc.* **1940**, *35*, 180−185.
(56) Schuck, P. J.; Fromm, D. P.; Sundaramurthy, A.; Kino, G. S.; Moerner, W. E. Improving the Mismatch between Light and Nanoscale Objects with Gold Bowtie Nanoantennas. *Phys. Rev. Lett.* **2005**, *94* (1), 017402.
(57) Johnson, P. B.; Christy, R. W. Optical Constants of the Noble Metals. *Phys. Rev. B* **1972**, *6* (12), 4370−4379.
(58) Brown, L.; Koerner, T.; Horton, J. H.; Oleschuk, R. D. Fabrication and Characterization of Poly(methylmethacrylate) Microfluidic Devices Bonded Using Surface Modifications and Solvents. *Lab Chip* **2006**, *6* (1), 66−73.
(59) Turkevich, J.; Stevenson, P. C.; Hillier, J. A Study of the Nucleation and Growth Processes in the Synthesis of Colloidal Gold. *Discuss. Faraday Soc.* **1951**, *11*, 55−75.